Laser-induced cooperative transition in molecular electronic crystal

*Yong Hu, Dasharath Adhikari, Andrew Tan, Xi Dong, Taishan Zhu, Xiaoyu Wang, Yulong Huang, Travis Mitchell, Ziheng Yao, Nathan Dasenbrock-Gammon, Elliot Snider, Ranga P. Dias, Chuankun Huang, Richard Kim, Ian Neuhart, Ahmed H. Ali, Jiawei Zhang, Hans A. Bechtel, Michael C. Martin, Stephanie N. Gilbert Corder, Feng Hu, Zheng Li, Jason N. Armstrong, Jigang Wang, Mengkun Liu, Jason Benedict, Eva Zurek, Ganapathy Sambandamurthy, Jeffrey C. Grossman, Pengpeng Zhang, Shenqiang Ren**

Y.Hu, Y. Huang, F. Hu, Z. Li, Prof. J.N. Armstrong, Prof. S.Q. Ren
Department of Mechanical and Aerospace Engineering
University at Buffalo, The State University of New York
Buffalo, NY 14260, USA
Email: shenren@buffalo.edu

D. Adhikari, A.H. Ali, Prof. G. Sambandamurthy
Department of Physics,
University at Buffalo, The State University of New York
Buffalo, NY 14260, USA

A. Tan X. Dong Prof. P. P. Zhang
Department of Physics and Astronomy
Michigan State University
East Lansing, MI 48824, USA

T.S. Zhu Prof. J.C. Grossman
Department of Materials Science and Engineering
Massachusetts Institute of Technology
Cambridge, MA 02139, USA

X.Y. Wang, T. Mitchell, J. Benedict, Prof. E. Zurek
Department of Chemistry
University at Buffalo, The State University of New York
Buffalo, New York 14260, USA

Z.H. Yao, J.W. Zhang, Prof. M.K. Liu,
Department of Physics and Astronomy
Stony Brook University
Stony Brook, NY 11794, USA

Z.H. Yao, H.A. Bechtel, M.C. Martin S.G. Corder
Advanced Light Source Division
Lawrence Berkeley National Laboratory
Berkeley, CA 94720, USA

N. Gammon, Prof. R.P. Dias
Department of Physics & Astronomy
University of Rochester
Rochester, New York 14627, USA

N. Gammon, E. Snider, Prof. R.P. Dias
Department of Mechanical Engineering
University of Rochester
Rochester, New York 14627, USA

C. Huang, R. Kim, Prof. J.G. Wang
Department of Physics and Astronomy and Ames Laboratory-U.S. DOE
Iowa State University
Ames, Iowa 50011, USA

Prof. S.Q. Ren
Research and Education in Energy Environment & Water Institute
University at Buffalo
The State University of New York, Buffalo, NY 14260, USA

Keywords: hidden phase, bistability, photoexcitation, dimerization, DFT calculations.

Abstract

The competing and non-equilibrium phase transitions, involving dynamic tunability of cooperative electronic and magnetic states in strongly correlated materials, show a great promise in quantum sensing and information technology. To date, the stabilization of transient states is still in the preliminary stage, particularly with respect to molecular electronic solids. Here we demonstrate a dynamic and cooperative phase in potassium-7,7,8,8-tetracyanoquinodimethane (K-TCNQ) with the control of pulsed electromagnetic excitation. Simultaneous dynamic and coherent lattice perturbation with 8ns pulsed laser (532 nm, 15 MW/cm^2, 10Hz) in such a molecular electronic crystal initiates a stable long-lived (over 400 days) conducting paramagnetic state (~ 42 Ωcm), showing the charge-spin bistability over a broad temperature range from 2 to 360 K. Comprehensive noise spectroscopy, in-situ high pressure measurement, electron spin resonance (ESR), theoretical model and scanning tunneling microscopy/spectroscopy (STM/STS) studies provide further evidence that such an transition is cooperative, requiring a dedicate charge-spin-lattice decoupling to activate and subsequently stabilize non-equilibrium phase. The cooperativity triggered by ultrahigh-strain-rate (above 10^6/s) pulsed excitation offers a collective control towards the generation and

stabilization of strongly correlated electronic and magnetic orders in molecular electronic solids and offers unique electro-magnetic phases with technological promises.

1. Introduction

Photoinduced phase transformations in strongly correlated materials occur when non-equilibrium breaking and transforming electronic and/or structural orders takes place, showing promise in quantum sensing and information technology.[1-8] The photoinduced states, such as light-induced superconductivity and ferroelectricity,[1-3, 8] are of fundamental interest as they offer a unique window into the regime of strongly coupled degrees of freedom in a material and novel functionality absent in equilibrium states.[5] However, photoinduced states of matter are often transient and the system reverts promptly to the ground state through electronic and lattice relaxation process, becoming the long-standing obstacle to dynamically tune and stabilize the metastable phases.[1-3, 6, 9] Here, we hypothesize an equilibrium conducting phase can be realized if the relaxation path can be altered by dynamic lattice perturbation at a characteristic timescale of electron-phonon decoupling.[10-12] Pulsed electromagnetic excitation provides a pathway to access both photoexcitation and ultrahigh strain-rate effects,[13-15] and their synergistic interplay made it possible to realize stable hidden conducting phase.

Quasi-one dimensional molecular crystals with spin-Peierls transition, like alkali metal TCNQ complexes[16] and (tetramethyltetrathiofulvalene)$_2$PF$_6$[17], are potential model systems due to their strong electron-phonon coupling. We select K-TCNQ to study the cooperative behavior in molecular electronic crystal due to its high critical temperature (T_c, ~395 K) for spin-Peierls transition. In K-TCNQ, the localized π electron on the TCNQ site forms an anion radical ($TCNQ^-$) and the system undergoes spin-Peierls transition with the formation a diamagnetic insulating singlet ground state.[11, 12] We obtain its structural packing motif through the scanning tunneling microscopy (STM) and single crystal crystallography, where K atoms

occupy the center sites of the TCNQ mesh (**Figure 1**a and Figures S1-S4). As a result of pulsed electromagnetic irradiation, photoexcitation could melt the electronic ordering in the spin-Peierls state at room temperature,[11, 18] while its ultrahigh-strain-rate effect works cooperatively to uncover a hidden conducting phase (Figures 1b-1c). In addition, we found that delicately tuning the laser pulses with power and repetition rate (frequency) could modify the degree of electronic ordering and realize quasi-stable states. The in-situ and atomic-scale mechanistic studies, experimentally and theoretically, suggest the crucial role of ultrahigh-strain-rate effect on such non-equilibrium electronic-disordered (electronic glass) phase transition, wherein a switchable magneto-electronic bistability can be achieved from 2 to 360 K.[19-24] The strong cooperativity among electronic and lattice degrees leads the system towards an equilibrium hidden state, which exhibits distinct electronic and magnetic properties (Figure 1d) that remain stable for over 400 days, significantly extending the lifetime of photoinduced transient state.

2. Results

The self-assembled K-TCNQ crystal shows an insulating-to-conducting phase transition driven by pulsed electromagnetic irradiation along the stacking *a*-axis. As shown in **Figure 2**a, laser pulse L_1 (15 MW/cm^2 at 10 Hz repetition rate) triggers such transition characterized by an abrupt resistivity drop by four orders of magnitude to ~ 42 Ωcm. As shown in Figure 2a (left), each pulse induces the resistivity drop while a stable low resistivity state can be achieved after multiple pulse treatment, suggesting the cumulative and cooperative effect in the transition. Moreover, the resistivity perpendicular to the stacking *a*-axis during the laser irradiation (Figure 2b) maintains its insulating behavior, confirming its one-dimensional nature (Figure 2b). Such cooperative conducting state can be maintained and lasted over 400 days (Figure 2c) in the treated crystal. In addition, time dependent electrical resistivity of the conducting phase shows its stability over a wide temperature range (2 - 360 K, Figure S6). It

should also be noted that the reversible nature (Figure S8) of the transition can be activated with the application of a higher-power laser pulse excitation (50 MW/cm^2 at 1 Hz repetition rate, the right panel of Figure 2a).

The ultrahigh strain rate and photoexcitation of pulsed irradiation[13, 25, 26] play an important role in the conducting phase transition of K-TCNQ, and therefore we systematically modulate the pulse power and its repetition rate (frequency) on its resistivity (**Figure 3**a). By increasing pulse power, both photoexcitation as well strain effects should become more obvious. The photoexcitation effects at higher power level normally have a tendency of decreasing the resistivity of K-TCNQ. Thus, if photoexcitation effect is dominant, we should realize conducting state with higher power pulses even at lower repetition rate. However, our experimental observations are not supporting it suggesting pressure effect should be dominant at lower pulse repetition rate. This indicates the pressure due to laser pulses would be playing significant role in achieving and breaking the stable conducting phase. To further corroborate the ultrahigh strain rate induced pressure effect, we design and carry out the in-situ electrical resistance measurement under the pressure (Figure 3b). The relaxation of photoexcited states in K-TCNQ depend critically on its lattice distortion. In-situ Raman spectra of K-TCNQ under pressure (Figure 3b) shows that C=CN wing stretching mode[27] shifts to a higher frequency, resulting the change in the crystal and electronic structure, which suggests the possible role of ultrahigh strain-rate effect in the transition. The thermal effect can be ruled out as the conducting state cannot be obtained with the increase of the temperature.[28]

Previous studies suggest the dimerized phase in K-TCNQ could be melted transiently and its recovery occurs in ultrafast time scale,[11, 12, 18] while high-strain-rate pulsed laser induced conducting phase can be stable.[11] In this study, based on the observations, we conjecture the effects of photoexcitation and ultrahigh strain rate would work in a synergistic way to achieve the equilibrium conducting state. The pulsed-laser photoexcitation triggers the transient

melting of dimerized phase and generates ultrahigh-strain-rate in K-TCNQ,[11-13, 18, 25, 26] preventing electron relaxation towards the ground state. Instead, the symmetry-broken ground state follows a trajectory to a state that is not accessible or does not exist under thermal equilibrium, and thus a reversible hidden conducting phase can be achieved.

To provide a microscopic understanding of such cooperative phase transition, we implement a variety of in-situ spectroscopy and mechanistic modeling studies. After the L_1 pulse treatment, a new characteristic Raman vibrational mode appears at 1,453 cm^{-1} for the charge sensitive C=CN wing stretching band, suggesting the formation of K^0-$TCNQ^0$ phase (**Figure 4**a),[27] signaling the change in electronic ordering. X-ray diffraction (XRD) patterns show the expansion of lattice in the conducting phase (Figure 4b), suggesting the electronic and lattice degree of freedom are strongly coupled in K-TCNQ. In Figure 4c, the normalized Power Spectral Density (PSD) of the resistance fluctuation at different resistivity are presented using resistance noise spectroscopy.[29, 30] The PSD for high resistivity state follows ubiquitous $1/f^{\alpha}$ (frequency exponent(α) ~ 1) dependence, and the normalized PSD magnitude increases by several orders as we traverse towards the conducting states. Furthermore, frequency exponent (α) increases from expected homogenous phase value (~1) (Figure 4d),[30, 31] suggesting the phase-mixing enhanced slow charge dynamics in the laser-driven phase. The trends observed in both the normalized PSD and the frequency exponent suggest laser-pulse-induced conducting state is an electrically inhomogeneous phase.[32-34] The charge-transfer[11, 12, 18] and charge redistribution in K-TCNQ could occur in the conducting phase transition.

The conducting regions can be formed at the phase boundaries with different charge transfer states.[35, 36] A molecular heterojunction of TCNQ and K-TCNQ is therefore constructed and examined by scanning tunneling microscopy/spectroscopy (STM/STS). The single-layer K-TCNQ shows the same packing structure as that of K-TCNQ crystal. The STS spectra taken near the heterojunction of TCNQ and K-TCNQ are shown in Figure 4e with the morphology

of the area illustrated in the inset. Here, K doping is primarily localized on the edges of the TCNQ assembly. By tracking the spectral feature located at ~0.6 V, we find that this peak broadens and moves towards the Fermi level from TCNQ, the interface of TCNQ/K-TCNQ, to K-TCNQ. The movement of the peak towards the Fermi level is associated with the electron population in TCNQ as a result of the K doping. The charge inhomogeneity due to charge redistribution after laser treatment is examined by computationally creating a K vacancy in unit cell of K_7TCNQ_8 (Figure 4f). The charge density is alternatively increased and decreased on the molecular dimers due to the presence of K vacancy, while the density of states (DOS) suggests an improved electrical conductivity after laser treatment.

The interplay of charge, spin, orbital and lattice degrees of freedom in K-TCNQ play a crucial role in phase transition and cooperativity. As shown in **Figure 5**a, laser driven electronic bistability in K-TCNQ is shown from 2 to 360 K. The conducting phase is paramagnetic from its electron spin resonance (ESR, Figure 5b), suggesting the conducting paramagnetic phase switched from the insulating diamagnetic singlet phase due to the strong coupling of charge, spin and lattice degrees. The magnetic state can also be maintained over the same temperature regime (2-360 K). It should be mentioned that the pristine K-TCNQ exhibits insulating behavior over the entire temperature regime below and above T_c without showing bistability. Thus, the achieved bistability is hidden from a dimerized phase, as the dimerization is thought to be unfavorable for developing conducting or magnetic molecular solids.[21] The laser-induced phase transition in K-TCNQ simultaneously activates its magneto-electronic bistability from 2 to 360 K, a broad bistability temperature range among the reported molecular crystals (Figure 1d). It should be mentioned that the laser-driven hidden state is different from the hidden phases reported in spin crossover materails.[24, 37] In K-TCNQ, the hidden bistability is achieved by dedicatedly breaking charge-spin-lattice coupling with high-strain-rate and photoexcitation effects from pulsed electromagnetic irradiation.

3. Conclusion

Our study reveals the dynamic control of electronic ordering in molecular electronic K-TCNQ crystal with pulsed electromagnetic irradiation, allowing for the emergence of a switchable and cooperative phase transition at room temperature. The cooperative photoexcitation and ultrahigh strain rate effects induce the dynamic perturbation on electron and phonon decoupled state to activate and stabilize electronic disordered conducting phase, on which a comprehensive mechanistic understanding is provided from molecular level. In addition to initiate an equilibrium long-lived (over 400 days) electronic disordered phase, we demonstrate a simultaneous charge-spin bistability covering a broad temperature regime from 2 to 360 K. The findings shown here pave the way to utilize pulsed laser to uncover cooperative phase transition in molecular electronic solids, encompassing the emergent effects and hidden phases like light-induced superconductivity, and ferroelectricity, etc.

4. Experimental Section

Large size K-TCNQ synthesis: K-TCNQ single crystals were prepared in acetonitrile by combining the slow cooling and evaporation method. Potassium iodide (150 mg, 0.904 mmol), TCNQ (183 mg, 0.893 mmol), and acetone (40 mL) were mixed in centrifuges at 473K water bath for 10 minutes. Small-size single crystals of reddish-purple needles were obtained after the solution was cooled slowly down to room-temperature. The obtained small single crystal powder was then purified at 423K in the chamber, which was evacuated by a cryo pump to a pressure of 1×10^{-7} torr. 100 mg purified K-TCNQ powder was dissolved in 400 mL acetonitrile solution in a beaker at 473K in a water bath for 30 minutes. Crystal growth was allowed to proceed for two days before harvesting. Reddish-purple needles were obtained with a typical size of 3 x 1 x 1 mm. These crystals grow preferentially along the *a*-axis. All the processes were

conducted in a fume hood. In order to get a large-size single crystal, the beaker must be very clean.

Small size K-TCNQ Synthesis: Small size (few μm) K-TCNQ was Synthesized for single crystal XRD analysis. Potassium iodide (17.1 mg, 0.103 mmol), TCNQ (20.5 mg, 0.100 mmol), and acetone (100 μL) were ground using a mortar and pestle. The reaction mixture quickly transitioned from a mix of golden-white powder to a greenish-purple paste. The paste was dissolved in a minimal amount of acetone, transferred to a 20 mL scintillation vial, and loosely capped. After slow evaporation, needles of K-TCNQ had formed and were mechanically separated from yellow prisms of TCNQ.

Laser specification

Q-switched laser (Beamtech Nimma-900, Beamtech China, Beijing, China, which operates at a wavelength of 532 nm with an adjustable energy and repetition rate from 1 to10 Hz is used for the study. The default pulse width of the Nimma-900 (8 ns) was used and diameter of the laser spot is 9 mm.

Electrical and magnetic transport measurements

Current-voltage (I-V) characteristics and both temperature and time dependence of electrical conductivity (or resistivity) measurements were performed in Quantum Design Physical Property Measurement System (PPMS) and JANIS ST-300T Compact Cryostats using a Keithley 2450 source meter. Magnetic susceptibility was measured using a Vibrating sample magnetometer (VSM) (MicroSense EZ7-380V) and PPMS vibrating sample magnetometer (PPMS VSM, Quantum Design).

High pressure study

High pressure in-situ resistance measurement was done using Diamond anvil cells (DACs). Type Ia diamonds (Almax) with 200 microns diameter culets and rhenium gaskets within custom DACs were used to apply pressure up to 11 GPa. The schematic of experimental setup was depicted in the inset of Figure 3b: samples were loaded into alumina packed DACs and

four platinum electrodes (~4 micron thick) were used. Keithley 2450 source meter was used to record sample resistance. Reported resistances and errors were the result of averaging the resistance measured in multiple configurations using different current values. Pressure was determined from the fluorescence of rubies that were co-loaded with the sample.[38]

High-pressure Raman spectroscopy study

As shown in Figure S11, a custom micro-Raman spectroscopy setup utilizing a Spectra Physics Millenia eV 532nm laser and an Andor Kymera 328i spectrometer with a Newton 920 CCD was used to capture the Raman spectra. Pressure was determined from the fluorescence of co-loaded pieces of ruby dust.[38]

Raman spectroscopy study

Raman microspectroscopy under atmospheric pressure was performed using a Renishaw inVia Raman microscope (Renishaw, Inc. Hoffman Estates, IL), equipped with a Leica DMLM microscope (5×, 20×, and L50× objectives). Spectra were collected using a Renishaw diode laser (488 nm, ≈2 μm × 2 μm irradiated area, 1200 l/m grating). The microstructure examination was performed in a field emission gun scanning electron microscope (JSM 7001F, Jeol).

Electron spin resonance (ESR) measurement

X-band Electron spin resonance (ESR) spectra were recorded on a Bruker 300 spectrometer equipped with a dual mode microwave cavity. The microwave frequency was calibrated with a frequency counter and the magnetic field with a gauss meter.

Scanning tunneling microscopy/spectroscopy (STM/STS) study

STM/STS studies were carried out in an ultrahigh vacuum (UHV) setup, using a commercial LT-Omicron scanning microscope operated at 77K. STM images were taken at constant current mode with a Pt-Ir tip. STS acquisition was achieved with lock-in technique. Typical modulation bias and frequency were 26 mV and 1 kHz respectively. Spectra on Ag(111) were taken periodically as a reference to confirm tip consistency. The Cu(111) surface was cleaned by repeated ion sputter cycles at 2keV, ~30uA. The deposition of TCNQ was carried out using a

valved thermal evaporator. To study K-doped TCNQ, a separate potassium dispenser from SAES was used to controllably dope pre-grown TCNQ samples with K atoms.

Noise spectroscopy measurement

Low-frequency resistance noise spectroscopy was performed using an AC Wheatstone bridge method[39, 40]. The Wheatstone bridge was typically used for resistance of the order of 10 - 100 kohm and for a higher resistance case DC technique is used.[41, 42] The 7265 Dual-Phase DSP Lock-In Amplifier enables to collect both in-phase and out-of-phase fluctuation signals simultaneously. With the proper selection of the ac excitation frequency (283.117 Hz in our case), the power spectral density (PSD) of sample resistance fluctuation was obtained by subtracting out-of-phase PSD from in-phase PSD.[39, 43] An analog-to-digital converter was used for signal digitization and data was collected at a specific sampling rate (256 samples/s. For each measurement the signal was recorded for approximately half an hour and repeated several times. Three-stage signal decimation was employed for signal downsampling and Welch Periodogram method was used to estimate PSDs.[44] In order to eliminate undesired spurious signals care is taken and special shielding and grounding of experiments are made.

***Ab Initio* calculations based on density functional theory**

The structural and electronic calculations were done using density functional theory (DFT) implemented in the Vienna Ab-initio Simulation Package (VASP).[45, 46] A unit cell consisting of 8 chemical units, $[K(C_3NH)_4]_8$ was adopted for structural relaxation and electron band structure calculations. Projector-augmented wave (PAW) potentials[47] were employed with a 520 eV energy cutoff and the following valence electrons were treated explicitly ($3p^6\,4s^1$) for K, ($2s^2 2p^3$) for N, ($2s^2 2p^2$) for C, and ($1s^1$) for H. The first Brillouin zone was sampled by the tetrahedron method on a Monkhorst-Pack scheme,[48] with a $4 \times 4 \times 4$ *k*-mesh. All structures were relaxed until the force on each atom was less than 0.01 meV/Å. The electronic density of states and band structures were calculated with the B3LYP hybrid functional[49] which is known to successfully predict a wide range of properties for molecular systems.

The PBE band structure was shown in Figure S13, and the charge density plot was shown in Figure S14. The conduction band minimum (CBM) and valence band maximum (VBM) were located at the high-symmetry M and L points, which were included in the B3LYP band gap calculations.

Single crystal X-ray diffraction experimental methods:

A single crystal suitable for X-ray diffraction (XRD) was mounted on the tip of a glass fiber with oil and placed on a Bruker SMART APEX II CCD diffractometer installed at a rotating anode source (Mo-Kα radiation, λ = 0.71073 Å) with a detector-to-crystal distance of 40.00 mm and a 2θ-angle of 0 °. Frames were collected using five 180 ° ω-scans (0.5 ° scan width) at different φ-angles (φ = 0 to 288 ° at 72 ° increments) for a total of five runs and 1800 frames, nominally covering complete reciprocal space. The crystal was kept at 296.15 K during data collection. Data reduction was completed using SAINT version 8.38A, and a multi-scan absorption correction was applied using SADABS version 2016 included in the Bruker APEX3 software suite. Space-group determination was performed using the XPREP utility included in the SHELXTL software package. Using Olex2, the structure was solved with ShelXT using intrinsic phasing and refined using ShelXL using least squares minimization (full-matrix least-squares on F^2). Hydrogen atoms were placed in idealized positions and refined using a riding model.

Structure and elemental analysis

The crystal structure was characterized by X-ray diffraction (XRD; Rigaku Ultima IV instrument operating with a CuKa radiation) and Hitachi S4000 Field Emission Scanning Electron Microscope (FESEM) with IXRF Energy-dispersive X-ray Spectrometer (EDS). Fourier transform infrared spectroscopy (FTIR) was performed by using Agilent Cary 630 FTIR spectrometer.

Supporting Information

Supporting Information is available from the Wiley Online Library or from the author.

Acknowledgements

Y.H. and D.A. contributed equally to this work. Work at the University at Buffalo (S.R.) was supported by the U.S. Department of Energy, Office of Basic Energy Sciences, Division of Materials Sciences and Engineering, under Award DE-SC0018631 (Physical properties of molecular electronic crystals). The U.S. Army Research Office supports S.R. under Award W911NF-18-2-0202 (Self-assembly of organic crystals). STM/STS studies were supported by the U.S. Department of Energy (DOE), Office of Basic Energy Sciences, Division of Materials Sciences and Engineering under Award Number DE-SC0019120. X.W. and E.Z. thank the Center for Computational Research (CCR) at the University at Buffalo for providing computational resources.[50] E. Z. acknowledges the National Science Foundation (DMR-1827815) for financial support. Noise spectroscopy studies were supported by the National Science Foundation under award NSF-DMR 1726303. This work was supported by the Ames Laboratory, the US Department of Energy, Office of Science, Basic Energy Sciences, Materials Science and Engineering Division under contract #DE-AC02-07CH11358 (THz spectroscopy). This research used beamline 1.4 at the Advanced Light Source, which is a DOE Office of Science User Facility under contract no. DE-AC02-05CH11231. Z.H.Y acknowledges the partial support from the ALS Doctoral Fellowship in Residence Program. Work performed by Jason B. Benedict and Travis B. Mitchell was supported by: National Science Foundation, Directorate for Mathematical and Physical Sciences (award No. DMR-1455039).

Received: ((will be filled in by the editorial staff))
Revised: ((will be filled in by the editorial staff))
Published online: ((will be filled in by the editorial staff))

References

[1] T. Nova, A. Disa, M. Fechner, A. Cavalleri, *Science* **2019**, *364*, 1075.
[2] X. Li, T. Qiu, J. Zhang, E. Baldini, J. Lu, A. M. Rappe, K. A. Nelson, *Science* **2019**, *364*, 1079.
[3] M. Mitrano, A. Cantaluppi, D. Nicoletti, S. Kaiser, A. Perucchi, S. Lupi, P. Di Pietro, D. Pontiroli, M. Ricco, S. R. Clark, D. Jaksch, A. Cavalleri, *Nature* **2016**, *530*, 461.
[4] J. Zhang, X. Tan, M. Liu, S. W. Teitelbaum, K. W. Post, F. Jin, K. A. Nelson, D. Basov, W. Wu, R. D. Averitt, *Nat. Mater.* **2016**, *15*, 956.
[5] D. Mihailovic, *Nat. Mater.* **2016**, *15*, 930.
[6] L. Stojchevska, I. Vaskivskyi, T. Mertelj, P. Kusar, D. Svetin, S. Brazovskii, D. Mihailovic, *Science* **2014**, *344*, 177.
[7] H. Ichikawa, S. Nozawa, T. Sato, A. Tomita, K. Ichiyanagi, M. Chollet, L. Guerin, N. Dean, A. Cavalleri, S.-i. Adachi, *Nat. Mater.* **2011**, *10*, 101.
[8] E. Collet, M.-H. Lemée-Cailleau, M. Buron-Le Cointe, H. Cailleau, M. Wulff, T. Luty, S.-Y. Koshihara, M. Meyer, L. Toupet, P. Rabiller, *Science* **2003**, *300*, 612.
[9] V. Stoica, N. Laanait, C. Dai, Z. Hong, Y. Yuan, Z. Zhang, S. Lei, M. McCarter, A. Yadav, A. R. Damodaran, *Nat. Mater.* **2019**, *18*, 377.
[10] D. S. Ivanov, L. V. Zhigilei, *Phys. Rev. B* **2003**, *68*, 064114.
[11] H. Okamoto, K. Ikegami, T. Wakabayashi, Y. Ishige, J. Togo, H. Kishida, H. Matsuzaki, *Phys. Rev. Lett.* **2006**, *96*, 037405.
[12] T. Ishikawa, R. Hosoda, Y. Okimoto, S. Tanaka, K. Onda, S. Koshihara, R. Kumai, *Phys. Rev. B* **2016**, *93*, 195130.

[13] H. Gao, Y. Hu, Y. Xuan, J. Li, Y. Yang, R. V. Martinez, C. Li, J. Luo, M. Qi, G. J. Cheng, *Science* **2014**, *346*, 1352.
[14] M. Lejman, G. Vaudel, I. C. Infante, P. Gemeiner, V. E. Gusev, B. Dkhil, P. Ruello, *Nat. Commun.* **2014**, *5*, 4301.
[15] K. T. Ramesh, *Handbook of experimental solid mechanics* **2008**, *933*.
[16] Y. Takaoka, K. Motizuki, *J. Phys. Soc. Jpn.* **1979**, *47*, 1752.
[17] P. Foury-Leylekian, D. Le Bolloc'h, B. Hennion, S. Ravy, A. Moradpour, J.-P. Pouget, *Phys. Rev. B* **2004**, *70*, 180405.
[18] S. Koshihara, Y. Tokura, Y. Iwasa, T. Koda, *Phys. Rev. B* **1991**, *44*, 431.
[19] W. Fujita, K. Awaga, *Science* **1999**, *286*, 261.
[20] M. Itkis, X. Chi, A. Cordes, R. Haddon, *Science* **2002**, *296*, 1443.
[21] R. G. Hicks, *Nat. Chem.* **2011**, *3*, 189.
[22] S. Venkataramani, U. Jana, M. Dommaschk, F. Sönnichsen, F. Tuczek, R. Herges, *Science* **2011**, *331*, 445.
[23] N. Hoshino, F. Iijima, G. N. Newton, N. Yoshida, T. Shiga, H. Nojiri, A. Nakao, R. Kumai, Y. Murakami, H. Oshio, *Nat. Chem.* **2012**, *4*, 921.
[24] O. Sato, *Nat. Chem.* **2016**, *8*, 644.
[25] M. Lejman, G. Vaudel, I. C. Infante, P. Gemeiner, V. E. Gusev, B. Dkhil, P. Ruello, *Nat. Commun.* **2014**, *5*, 1.
[26] O. Matsuda, M. C. Larciprete, R. L. Voti, O. B. Wright, *Ultrasonics* **2015**, *56*, 3.
[27] K. Truong, C. Carlone, *Phys. Rev. B* **1979**, *20*, 2238.
[28] R. Kumai, Y. Okimoto, Y. Tokura, *Science* **1999**, *284*, 1645.
[29] A. M. Alsaqqa, S. Singh, S. Middey, M. Kareev, J. Chakhalian, G. Sambandamurthy, *Phys. Rev. B* **2017**, *95*, 125132.
[30] A. A. Balandin, *Nat. Nanotechnol.* **2013**, *8*, 549.
[31] J. Brandenburg, J. Müller, J. A. Schlueter, *New J. Phys.* **2012**, *14*, 023033.
[32] B. Raquet, A. Anane, S. Wirth, P. Xiong, S. Von Molnar, *Phys. Rev. Lett.* **2000**, *84*, 4485.
[33] R. Merithew, M. Weissman, F. Hess, P. Spradling, E. Nowak, J. O'Donnell, J. N. Eckstein, Y. Tokura, Y. Tomioka, *Phys. Rev. Lett.* **2000**, *84*, 3442.
[34] V. Orlyanchik, M. Weissman, M. A. Torija, M. Sharma, C. Leighton, *Phys. Rev. B* **2008**, *78*, 094430.
[35] H. Alves, A. S. Molinari, H. Xie, A. F. Morpurgo, *Nat. Mater.* **2008**, *7*, 574.
[36] N. Reyren, S. Thiel, A. Caviglia, L. F. Kourkoutis, G. Hammerl, C. Richter, C. W. Schneider, T. Kopp, A.-S. Rüetschi, D. Jaccard, *Science* **2007**, *317*, 1196.
[37] T. Boonprab, S. J. Lee, S. G. Telfer, K. S. Murray, W. Phonsri, G. Chastanet, E. Collet, E. Trzop, G. N. Jameson, P. Harding, *Angew. Chem.* **2019**, *131*, 11937.
[38] E. Snider, N. Dasenbrock-Gammon, R. McBride, M. Debessai, H. Vindana, K. Vencatasamy, K. V. Lawler, A. Salamat, R. P. Dias, *Nature* **2020**, *586*, 373.
[39] J. H. Scofield, *Rev. Sci. Instrum.* **1987**, *58*, 985.
[40] A. Ghosh, S. Kar, A. Bid, A. Raychaudhuri, *arXiv preprint cond-mat/0402130* **2004**.
[41] M. Weissman, *Rev. Mod. Phys.* **1988**, *60*, 537.
[42] P. Dutta, P. Horn, *Rev. Mod. Phys.* **1981**, *53*, 497.
[43] J. Moon, A. F. Mohamedulla, N. O. Birge, *Rev. Sci. Instrum.* **1992**, *63*, 4327.
[44] P. Welch, *IEEE Trans. Audio Electroacoust.* **1967**, *15*, 70.
[45] G. Kresse, J. Furthmüller, *Phys. Rev. B* **1996**, *54*, 11169.
[46] G. Kresse, J. Furthmüller, *Comput. Mater. Sci.* **1996**, *6*, 15.
[47] P. E. Blöchl, *Phys. Rev. B* **1994**, *50*, 17953.
[48] A. D. Becke, *J. Chem. Phys* **1993**, *98*, 5648.
[49] W. Perger, *Chem. Phys. Lett.* **2003**, *368*, 319.

[50] *Center for Computational Research, University at Buffalo. Available online: http://hdl.handle.net/10477/79221*.
[51] D. A. Shultz, R. M. Fico, P. D. Boyle, J. W. Kampf, *J. Am. Chem. Soc.* **2001**, *123*, 10403.
[52] J. L. Brusso, O. P. Clements, R. C. Haddon, M. E. Itkis, A. A. Leitch, R. T. Oakley, R. W. Reed, J. F. Richardson, *J. Am. Chem. Soc.* **2004**, *126*, 14692.
[53] O. Jeannin, R. Clérac, M. Fourmigué, *J. Am. Chem. Soc.* **2006**, *128*, 14649.
[54] A. Dragulescu-Andrasi, A. S. Filatov, R. T. Oakley, X. Li, K. Lekin, A. Huq, C. Pak, S. M. Greer, J. McKay, M. Jo, *J. Am. Chem. Soc.* **2019**, *141*, 17989.
[55] S. K. Pal, P. Bag, A. Sarkar, X. Chi, M. E. Itkis, F. S. Tham, B. Donnadieu, R. C. Haddon, *J. Am. Chem. Soc.* **2010**, *132*, 17258.
[56] D. Bates, C. M. Robertson, A. A. Leitch, P. A. Dube, R. T. Oakley, *J. Am. Chem. Soc.* **2018**, *140*, 3846.
[57] T. Li, G. Tan, D. Shao, J. Li, Z. Zhang, Y. Song, Y. Sui, S. Chen, Y. Fang, X. Wang, *J. Am. Chem. Soc.* **2016**, *138*, 10092.

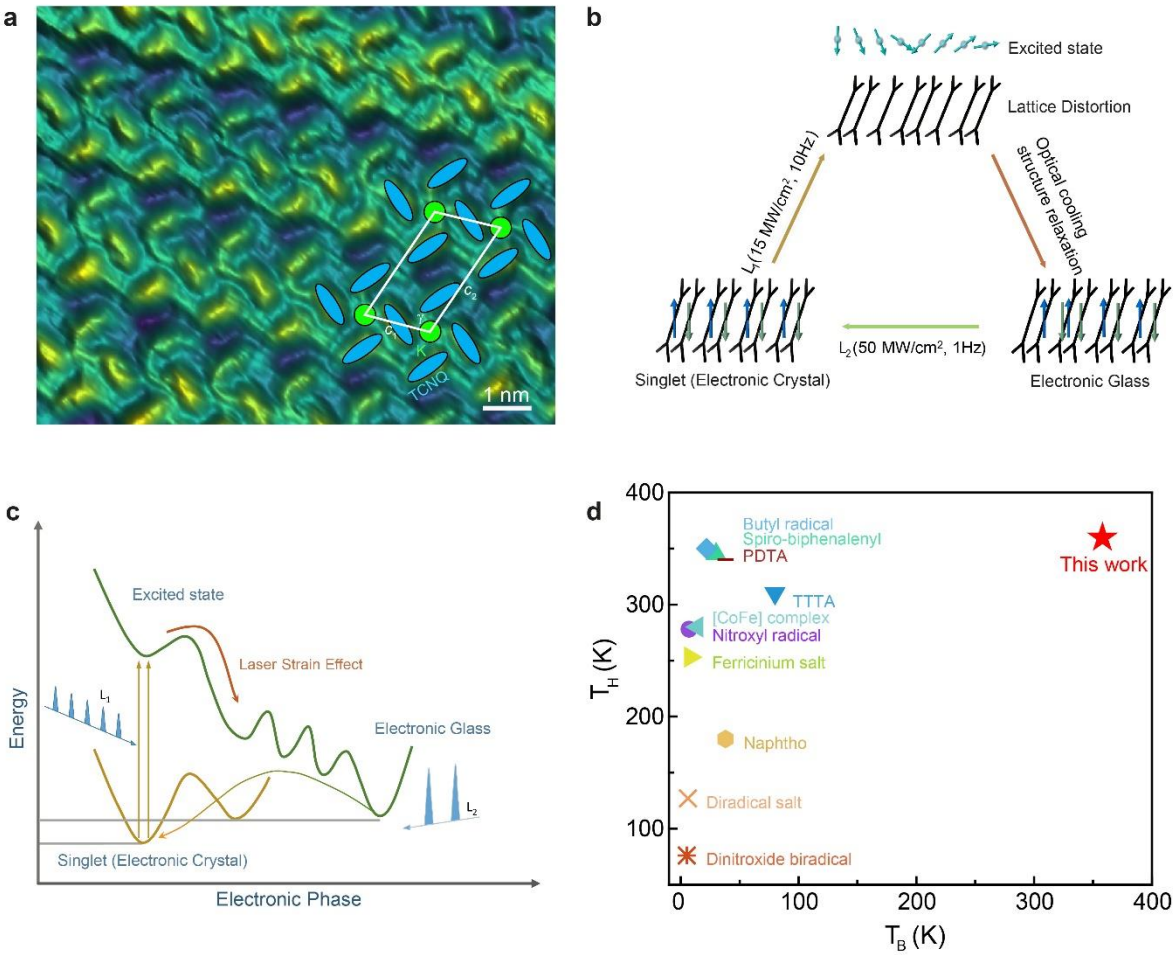

Figure 1. Crystal structure and electronic phase diagram for K-TCNQ. a) STM image of a striped phase of K-TCNQ with the stoichiometry ratio of 1:1. (Taken with a functionalized tip at V_s = 0.1 V, I_t = 30 pA). Note that TCNQ molecules are observed at empty-state imaging conditions while K atoms are observed in the filled-state imaging conditions. K atoms occupy the center of the TCNQ meshes, correlating to the packing motif in the b-c plane of the bulk crystal. The unit cell given by c_1=1.34 nm, c_2=2.40 nm, γ=107.91° is marked with the outline. b)-c), Schematic figure and energy diagram for a laser-driven electronic phase transition. The laser operates at a wavelength of 532 nm with an adjustable energy and repetition rate from 1 to 10 Hz. The pulse width is 8 ns. The diameter of the laser spot was 9 mm. L_1 (15 MW/cm^2, 10Hz, 76 mJ/pulse) can induce the melting of the singlet and form a disordered electron phase. As indicated, the laser pulse plays crucial role in the process. The achieved phase can break and recover the singlet phase through irradiation with a different laser pulse, L_2 (50 MW/cm^2, 1Hz, 254 mJ/pulse). Here, we define singlet state as an electronic crystal and the electronic disordered phase as an electronic glass. d) few selected switchable molecular crystals showing magnetic or magneto-electronic bistability. Bistable temperature regime: dinitroxide biradical (5 K),[51] PDTA (6 K),[52] [CoFe] complex (7 K),[23] ferricinium salt(8 K),[53] nitroxyl radical (14 K),[54] butyl radical (22 K),[55] spiro-biphenalenyl (30 K),[20] naphtho (38 K),[56] TTTA (80 K),[19] and diradical salt (127 K)[57]. Figure S5 shows the bistability in the thermal hysteresis phase transition, the system can have either of the two ground states at the same temperature. T_C: Phase transition temperature during cooling, T_H: Phase transition temperature during heating. T_B=T_H-T_C, bistability temperature range.

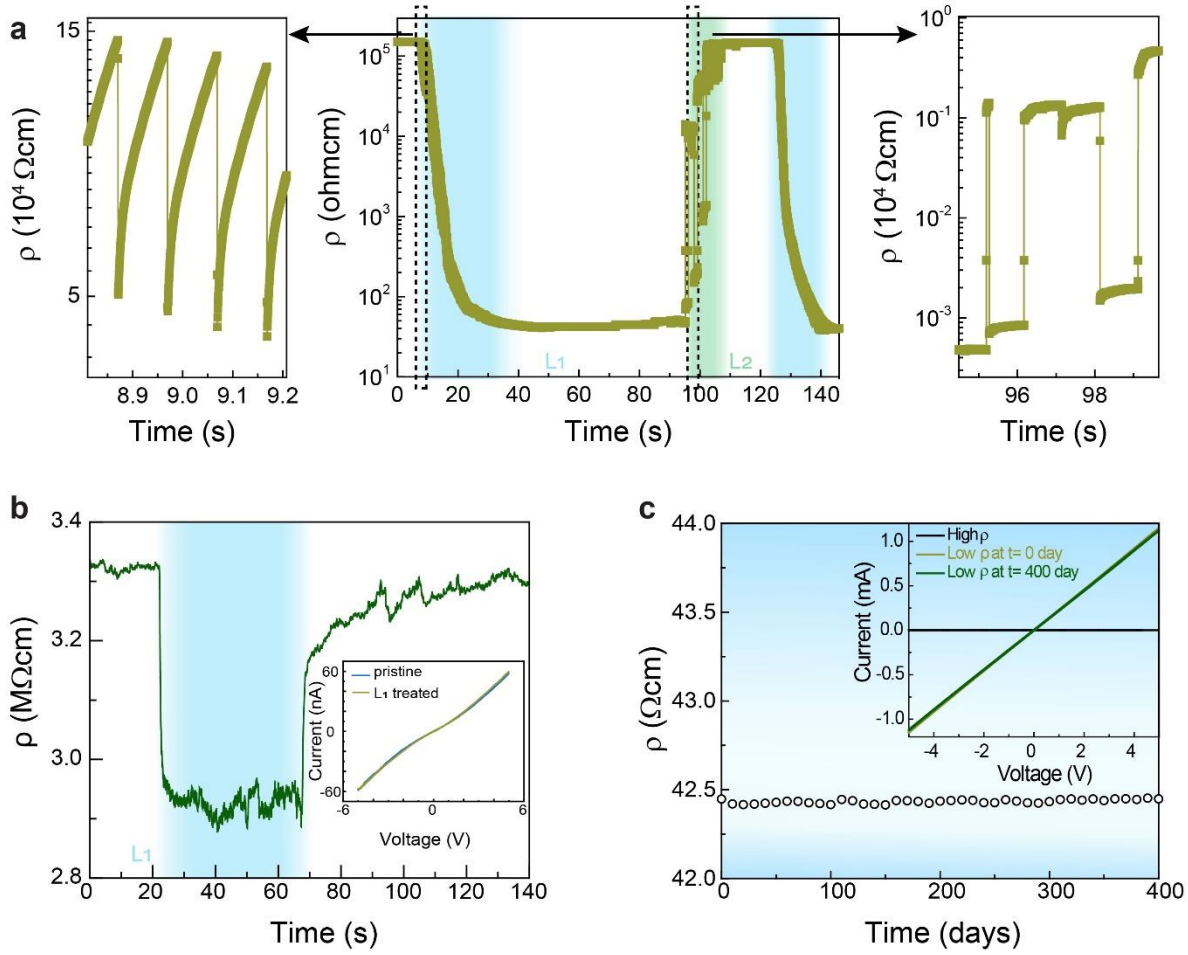

Figure 2. Laser driven reversible insulator to metal transition. a) Temporal profile of the sample electrical resistivity (ρ) during the laser pulse irradiations. Shadowed areas represent the laser treatment periods. Left and right-sided figures highlight the electrical resistivity evolution during the initial period of L_1 and L_2 pulse irradiations, respectively. b) Temporal profile of the sample electrical resistance perpendicular to *a*-axis direction during the L_1 laser pulse irradiations. Shadowed areas represent the laser treatment periods. Inset shows current-voltage (I-V) curves for the pristine (before L_1 treatment) and L_1 treated K-TCNQ sample perpendicular to a-axis direction. c) Performance indicative of the retention ability of the lowest-resistivity state for 400 days. Inset shows the I-V curves for the pristine K-TCNQ, L_1 pulse treated (t = 0 day), and (t = 400 days).

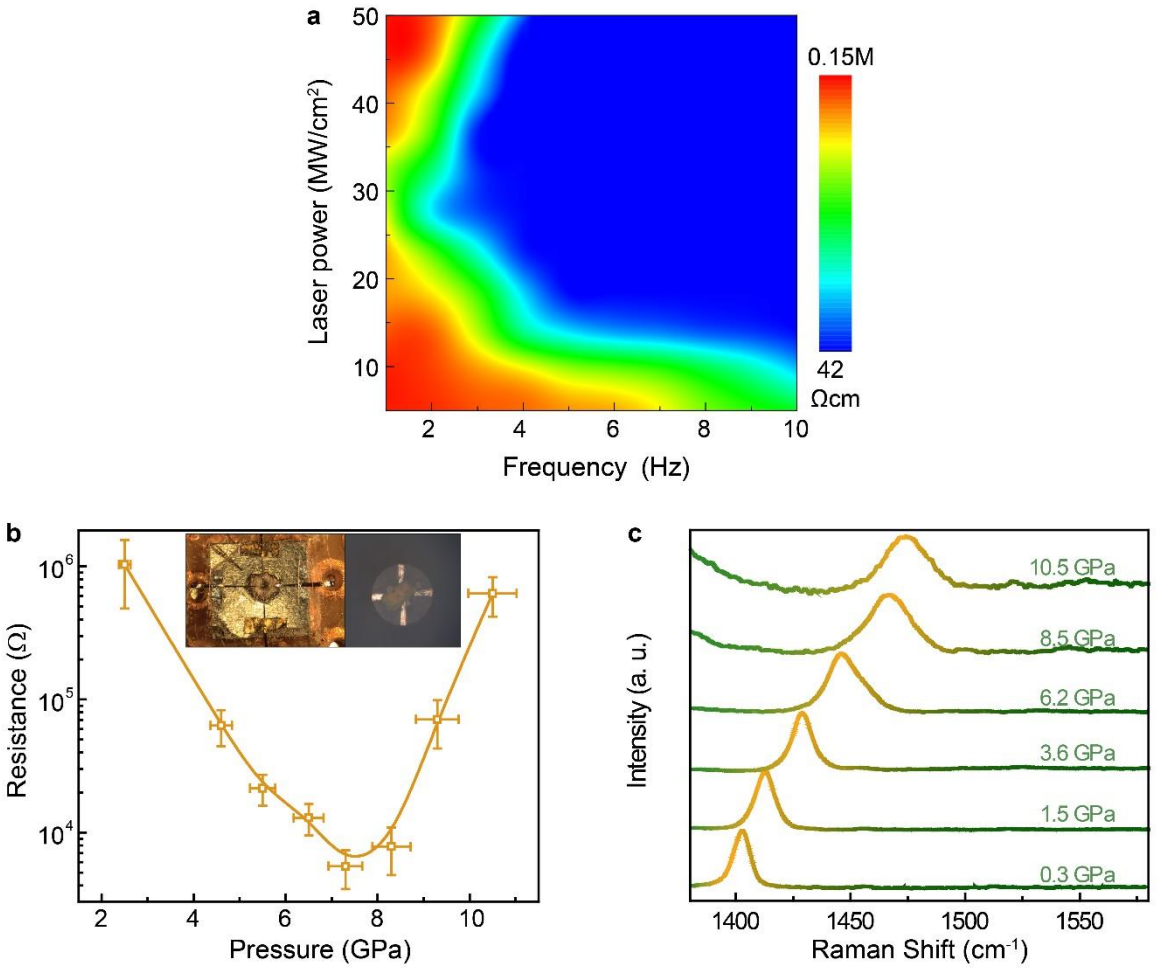

Figure 3. Laser driven transition and in-situ high pressure study. a) The color-plot represents the dependence of the resistivity on laser power and repetition rate (frequency), highlighting the importance of right combination of the two parameters to achieve the lowest electrical resistivity state. b) Pressure dependence of resistance for K-TCNQ. Inset shows the gasket setup used for the conductivity measurements. Four platinum electrodes, insulated from the rhenium gasket by tape, are shown with their tips placed into the sample chamber. The tips of the platinum electrodes making contact with the K-TCNQ sample, surrounded by insulating alumina. c) In-situ Raman spectra for K-TCNQ single crystal under different pressure.

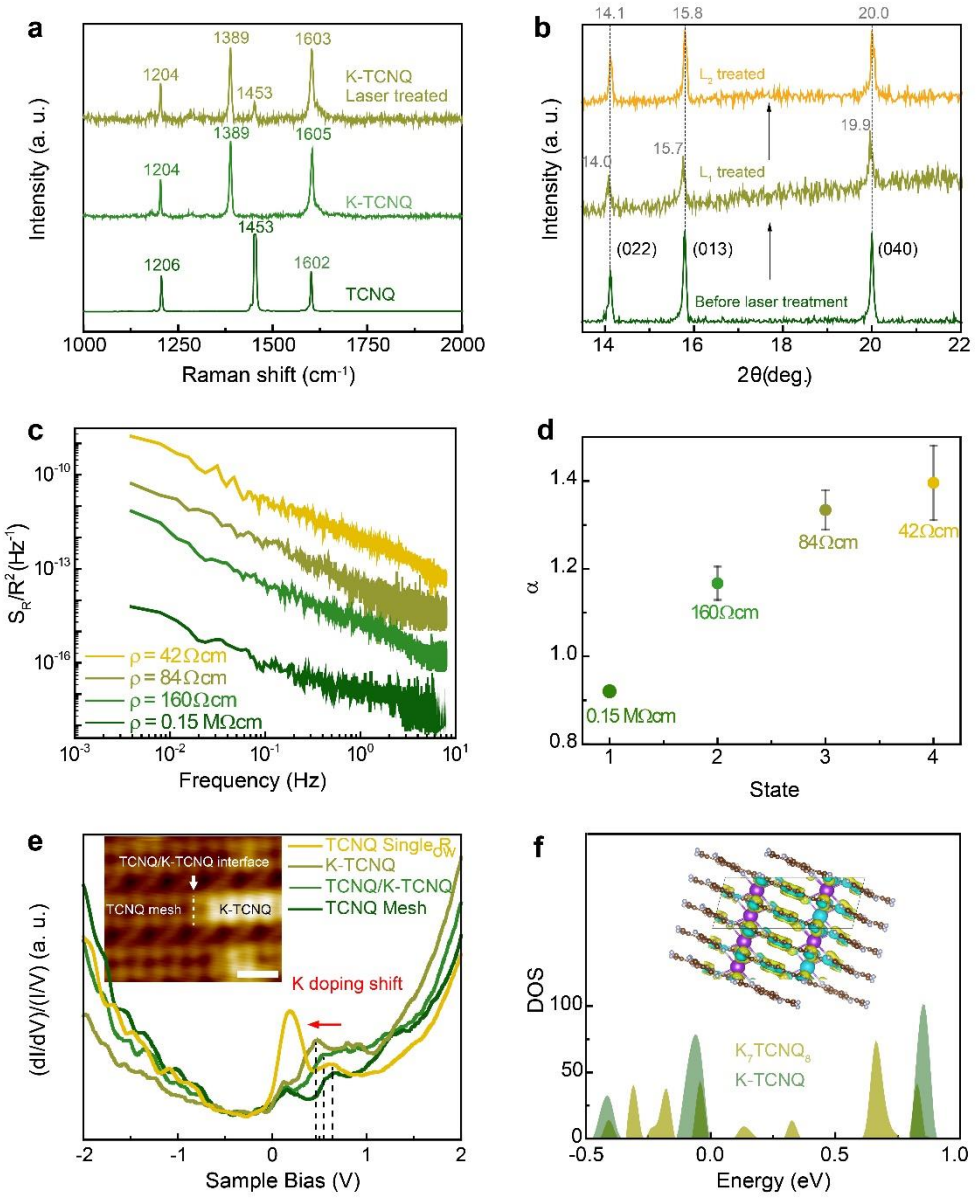

Figure 4. Conducting mechanism. a) Raman spectra for TCNQ, pristine K-TCNQ and L_1 treated K-TCNQ single crystal. b) XRD for K-TCNQ before laser treatment and after L_1, L_2 treatment. c) Normalized PSD of resistance fluctuation at several laser-induced low-resistivity states including the insulating phase. d) The frequency exponent (α) deviates significantly from its expected value ~ 1 in laser induced states suggesting the enhancement of slow charge dynamics resulting due to electrical inhomogeneity in the system. e) STS spectra (Vs = 2 V, It = 30 pA) taken on TCNQ or K-TCNQ molecules shown in the STM topological image in the inset (the scale bar is 2nm). f) Change in charge density due to the presence of one K vacancy in K_7TCNQ_8. Bottom figure shows the DOS for K_7TCNQ_8 and K-TCNQ.

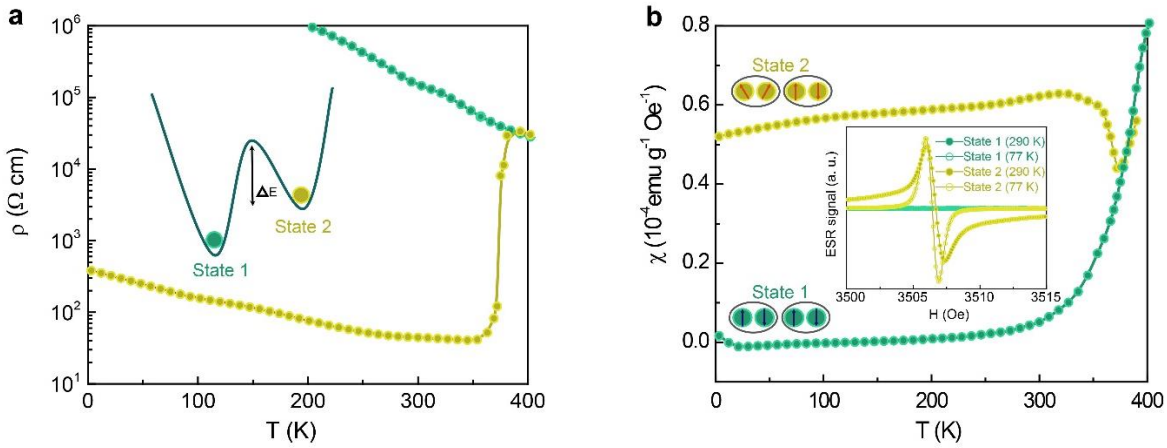

Figure 5. Tuning magneto-electronic coupling. a) Temperature dependence of electrical resistivity of K-TCNQ single crystals before (green color) and after (yellow color) L_1 treatment. Pristine K-TCNQ resistivity exhibits exponential temperature dependence. The resistivity of the laser-induced conducting phase increases slowly on cooling all the way down to 2 K. However, the state seems unstable at higher temperature and was maintained up to 360 K before switching back to the insulating phase. Inset shows schematic for two stable-insulating (State 1) and conducting (State 2) states which are separated by an energy barrier. b) Temperature dependence of magnetic susceptibility (χ) for state 1 (green color) and state 2 (yellow color). The laser induced magnetization was maintained from 2 K to 360K. Inset shows the ESR signals at room temperature (290 K) and liquid nitrogen temperature (77 K) from state 1 (green color) and state 2 (yellow color). The ESR signal becomes broad at 77 K, suggesting the reduced disorder with a decreasing temperature. The g-factors are 2.0266 and 2.0264 for 290 K and 77 K, respectively.

A major challenge in supramolecular electronic crystal is switchable control of its hidden phase. We have found the cooperative tuning of K-TCNQ through pulsed electromagnetic field into an emergent electronic disorder state, enabling the access to a long-lived (over 400 days) hidden conducting phase. A switchable magneto-electronic bistability is realized in a broad temperature range from 2 to 360 K.

Y. Hu, D. Adhikari, A. Tan, X. Dong, T. Zhu, X. T. Wang, Y.L. Huang, T. M., Z. H. Yao, N. D. Gammon, E. Snider, R. P. Dias, C. Huang, R. Kim, I. Neuhart, A. H. Ali, J. W. Zhang, H. A. Bechtel, M. C. Martin, S. N. G. Corder, F. Hu, Z. Li, J. N. Armstrong, J. G. Wang, M. K. Liu, J. Benedict, E. Zurek, G. Sambandamurthy, J. C. Grossman, P. P. Zhang, S. Q. Ren*

Laser-induced cooperative transition in molecular electronic crystal